# **Electronic Structures and Spectra of Donor-**

# **Acceptor Conjugated Oligomers**

Kiet A. Nguyen,<sup>a,b\*</sup> Ruth Pachter,<sup>a\*</sup> Lauren M. Loftus,<sup>a,c</sup> Gongyi Hong,<sup>a,b</sup> Paul N. Day,<sup>a,b</sup> Jason D. Azoulay,<sup>d</sup> Tod A. Grusenmeyer<sup>a</sup>

<sup>a</sup>Air Force Research Laboratory, Materials and Manufacturing Directorate
Wright-Patterson Air Force Base, OH 45433, USA

<sup>b</sup>UES, Inc., Dayton, OH, 45432 USA

<sup>c</sup>Azimuth Corporation, 2079 Presidential Dr. #200, Fairborn, OH 45342, USA

<sup>d</sup> School of Chemistry and Biochemistry and School of Materials Science and Engineering,
Georgia Institute of Technology, Atlanta, GA 30332, United States

<sup>\*</sup>Corresponding author

#### Abstract

Narrow bandgap donor-acceptor conjugated polymers offer new paradigms in photonics and optoelectronics owing to their chemical tunability, correlated electronic structures, and tunable open-shell electronic configurations. However, their extended electronic structures and structural and energetic heterogeneities challenge the development of rational theoretical approaches for predicting and describing emerging functionality. Here, we theoretically investigated prototypical narrow bandgap donor-acceptor conjugated oligomers comprised of alternating cyclopentadithiophene (CPDT) donors with benzothiadiazole (BT), benzoselenadiazole (BSe), benzobisthiadiazole (BBT), and thiadiazoloquinoxaline (TQ) acceptors. Density functional theory calculations of oligomers were carried out for up to ten repeat units and the structures, relative energies, singlet-triplet gaps, and absorption spectra were critically analyzed. For oligomers comprised of BT, BSe, and TQ acceptors, backbone curvature resulted in spiral structures which were energetically favored over their linear analogs. Circular dichroism spectra were calculated along with singlet-triplet splittings, indicating that this macromolecular topology results in better agreement with experimental singlet-triplet splittings. Oligomers with BBT-based acceptors preferred a linear geometry consistent with their openshell electronic structure. Based on the predicted low-energy conformations, one-photon absorption spectra calculations employing time-dependent density functional theory and the Tamm-Dancoff approximation, were shown to result in good agreement with the first absorption maxima of our measured experimental spectra. Furthermore, two-photon absorption maxima of the polymers could be correctly predicted, albeit the cross-sections were overestimated, which could be attributed to the level of theory employed or complex dependencies on macromolecular interactions and solution conformational changes.

#### I. Introduction

Although conjugated polymers have been studied for decades,<sup>1-3</sup> the development of donor-acceptor (DA) conjugated polymers (CPs) with very narrow bandgaps and open-shell electronic structures has only recently emerged.<sup>4-7</sup> These materials are of significant interest for photonics, spanning the infrared region of the electromagnetic spectrum, and in having large third-order nonlinear two-photon absorption responses, e.g., for open-shell systems.<sup>8</sup> Recent demonstrations<sup>9</sup> <sup>10</sup> <sup>11</sup> have shown that donor-acceptor CPs with large nonlinear optical two-photon absorption (TPA) cross-sections are promising for biomedical applications, including photodynamic therapy, drug delivery, and imaging.<sup>12-13</sup> Linear one-photon absorption (OPA) responses of these polymers find application for photodectectors<sup>14</sup> or organic solar cells.<sup>15-16</sup>

Recently, donor-acceptor CPs comprised of alternating cyclopentadithiophene (CPDT) and closely related bridgehead olefin (C=CPh) substituted donors, and acceptors based on 2,1,3-benzothiadiazole (BT),<sup>6</sup> 2,1,3-benzoselenadiazole (BSe),<sup>6</sup> benzo[1,2-*c*;4,5-*c*] bis[1,2,5]thiadiazole (BBT)<sup>17</sup> and 6,7-dimethyl[1,2,5]thiadiazolo[3,4-g]quinoxaline (TQ) heterocycles,<sup>6, 18</sup> have demonstrated linear photoresponses spanning the near infrared (NIR) to shortwave IR (SWIR). Previous density functional theory (DFT) studies on the corresponding oligomers determined structures, singlet-triplet splittings, and other properties by assuming linear chain conformations.<sup>6, 18 19</sup> To predict OPA responses, a computational time-dependent DFT (TD-DFT) study reported TD-B3LYP spectra for six model systems using CPDT-BT dimer model oligomers and derivatives, containing nitrogen and silicon in the bridgehead position of CPDT and substituting *N*-alkylthienopyrroledione for BT. While these calculations demonstrated good agreement with experimental measurements,<sup>20</sup> the success of the computational results was attributed to cancellation of errors resulting from the exchange-

represent the long-chain.<sup>20</sup> Subsequent calculations on oligomers of CPDT-BT containing seven repeat units using TD-DFT/B3LYP-6-311G(d) reported errors < 0.08 eV for vertical singlet excitation energies when compared to experimental values.<sup>21</sup> However, understanding the electronic and topological properties of donor-acceptor conjugated oligomers (DACOs) with narrower bandgaps, extended conjugation, stronger electronic correlations and open-shell electronic structures along with rational predictions of the electronic OPA and TPA responses employing well-benchmarked methods are lacking.

In this study, we report on the optical responses of long-chain oligomeric variants of DA CPs that comprise CPDT-based donors with 4,4-dimethyl-4*H*-cyclopenta[2,1-*b*:3,4-*b*]dithiophene (CPDT, Fig. 1a) and 4-(3,5-dimethylbenzylidene)-4*H*-cyclopenta[2,1-*b*:3,4-*b*]dithiophene (PhC=CPDT, Fig. 1b) donors and TQ, BT, BSe, BBT acceptors (Figure 1c-f). Solubilizing substituents on the donor were truncated to methyl groups (R = -CH<sub>3</sub>). Although considerable efforts have been devoted to benchmark DFT functionals for prediction of OPA and TPA properties, studies addressing the accuracy and efficient computation for long-chain oligomers remain nascent and are scant. Here, we benchmarked TD-DFT,<sup>22</sup> the Tamm-Dancoff approximation (TDA),<sup>23</sup> and the efficient simplified TDA (sTDA)<sup>24</sup> methods with different functionals against experimental OPA and TPA spectra.

Simulations on oligomers with up to 10 repeat units demonstrate that elucidation of the energetically favorable linear, curved, or twisted-chain macromolecular topologies can result in better agreement with experimentally measured singlet-triplet splittings in some cases. Such structures and their predicted electronic circular dichroism (ECD) spectra could motivate further macromolecular design and experimental characterization. Our well-benchmarked level of

theory based on these low-energy conformations are in good agreement with experimental absorption maxima ( $\lambda_{max}$ ), thereby paving the way for predictions of newly designed polymers. Moreover, TPA results agree with the experimentally determined TPA maxima, but cross-sections were overestimated. This could be attributed to the level of theory employed or complex dependencies on macromolecular interactions and solution conformations.

#### II. Methods

# A. Computational Details

Structural searches were carried out using Kohn-Sham (KS)<sup>25</sup> DFT with the B3LYP functional<sup>26-28</sup> and the long-range D3 dispersion energy of Grimme et al.<sup>29</sup> We applied the 6-31G(d,p) basis set for the atoms in the first three rows of the periodic table,<sup>30-31</sup> while for the Se atom, we used the Stuttgart/Dresden (SD) valence basis set and Effective Core Potential (ECP)<sup>32</sup> with two additional sets of *d*-functions ( $\zeta = 0.475412, 0.207776$ ).<sup>33</sup> DFT optimization, OPA and ECD calculations were performed using the Gaussian 16 program.<sup>34</sup> Quadratic response TPA calculations using resolution of identity (RI)<sup>35</sup> were performed with the TURBOMOLE program.<sup>36</sup> The corresponding linear<sup>24</sup> and quadratic<sup>37</sup> sTD and sTDA calculations were done using the sTDA program.<sup>38</sup> All excited state TD-DFT, TDA, and sTDA calculations were performed at the DFT structures using the same basis set as for the ground state calculations, and employing the B3LYP and PBE0<sup>39</sup> hybrid functionals, as well as the optimally tuned (OT)<sup>40</sup> range-separated hybrid (RSH) functional. OT-RSH functionals can improve errors for charge transfer (CT) excitations in molecules<sup>41</sup> and DACOs,<sup>42</sup> tuned for specific systems for more accurate results.

We consider the OT scheme<sup>40</sup> based on the CAMB3LYP<sup>43</sup> functional (OT-CAMB3LYP). The two-electron operator is partitioned into short-range (SR, first term) and long-range (LR, second term) terms as

$$r_{12}^{-1} = \frac{1 - \left[\alpha + \beta \cdot \text{erf}(\mu r_{12})\right]}{r_{12}} + \frac{\alpha + \beta \cdot \text{erf}(\mu r_{12})}{r_{12}}.$$
 (1)

The SR and LR terms are evaluated at the DFT and Hartree-Fock (HF) levels, respectively. For an asymptotically correct functional, the  $\alpha$  full-range and  $\beta$  long-range parameters are set to 0.2 and 0.8 ( $\alpha + \beta = 1$  instead of the original value  $\alpha$  of 0.19 and  $\beta$  of 0.46), respectively. The range-separation  $\mu$  parameter is tuned<sup>40</sup> to minimize the sum of the absolute differences between the highest occupied molecular orbital (HOMO) and the ionization potential (IP), and the lowest unoccupied molecular orbital (LUMO) and the electron affinity (EA).

To compare the OPA oscillator strengths to corresponding experimental extinction coefficients for ground (0) to excited state (e) transitions ( $f = \langle 0 | \mu | e \rangle$ ), where  $\mu$  is the electric dipole operator and  $f_{0f}(Q_i)$  is the oscillator strength for structure  $Q_i$ ), and considering a normalized Gaussian lineshape function, we use<sup>44</sup>

$$\varepsilon(\nu') = \frac{2\sqrt{\ln 2}}{4.32 \times 10^{-9} \sqrt{\pi}} \sum_{i} g_{i} \left(Q_{i}\right) \sum_{f} \frac{f_{0f}(Q_{i})}{\text{FWHM}} \exp\left[-4 \ln 2 \left(\frac{\nu' - \nu^{0f}(Q_{i})}{\text{FWHM}}\right)^{2}\right], \tag{2}$$

where  $g(Q_i)$ ,  $f_{0f}(Q_i)$ , and  $v^{0f}(Q_i)$  are the Boltzmann factor, oscillator strength, and transition frequency for a given  $Q_i$  isomer, respectively. FWHM is the full-width at half-maximum of the Gaussian line shape. Similarly, using the rotational strength expression  $(R = \text{Im}(\langle 0 | \mu | e \rangle \cdot \langle e | M | 0 \rangle)$ , M is the magnetic dipole operator) the ECD<sup>45</sup> spectral curve is obtained by as

$$\Delta \varepsilon \quad (\nu') = \frac{2\sqrt{\ln 2}}{2.296 \times 10^{-39} \sqrt{\pi}} \sum_{i} g_{i} \left(Q_{i}\right) \sum_{f} \frac{R_{0f}\left(Q_{i}\right)}{\text{FWHM}} \exp\left[-4\ln 2\left(\frac{\nu' - \nu^{f}}{\text{FWHM}}\right)^{2}\right], \tag{3}$$

where  $R_{0j}(Q_i)$  is the rotational strength for structure  $Q_i$ .

The degenerate TPA cross-section for linearly polarized photons with parallel polarization is obtained as

$$\delta \left(2E_{\lambda}\right) = \frac{16\pi^4}{c^2h} \left(\frac{\ln 2}{\pi}\right)^{1/2} E_{\lambda}^2 \sum_{i} g_i \left(Q_i\right) \sum_{f} \frac{\left|S_{0f}\left(Q_i\right)\right|^2}{(\text{FWHM})^2} \exp\left[-4\ln 2\left(\frac{2E - E_f}{\text{FWHM}}\right)^2\right],\tag{4}$$

where c is the speed of light, h is Planck's constant,  $E_{\lambda}$  is the photon energy, and  $S_{f0}$  is the two-photon matrix element for a two-photon transition between the ground- (0) and excited-state (f). The two-photon matrix elements were computed with quadratic response TD-DFT<sup>46</sup> and sTD.<sup>37</sup> TPA cross-sections are reported in GM<sup>47</sup> units (1 GM = 1 × 10<sup>-50</sup> cm<sup>4</sup> s photon<sup>-1</sup>molecule<sup>-1</sup>).

### **B.** Experimental Characterization

We synthesized poly(4-(4-(3,5-didodecylbenzylidene)-4*H*-cyclopenta[2,1-*b*:3,4-*b*]dithiophen-2-yl)benzo[*c*][1,2,5]thiadiazole, PhC=CPDT-BT) and poly(4-(4-(3,5-didodecylbenzylidene)-4*H*-cyclopenta[2,1-*b*:3,4-*b*]dithiophen-2-yl)benzo[*c*][1,2,5]selenadiazole, PhC=CPDT-BSe) as previously reported.<sup>48</sup> Solutions of the polymers at concentrations of 5 mg/mL (7 mM) for Z-scan measurements were made by dissolving the polymer in chlorobenze-d<sub>5</sub> (Sigma-Aldrich), sonicating, and stirring at 70 °C for 30 minutes. The solutions were then allowed to cool to room temperature before being filtered through a 0.2 μm PTFE syringe filter. A portion of these solutions were then diluted to a final concentration of 1 mg/mL (1.4 mM). The molar concentrations of these solutions are calculated from the molecular weight of the repeat unit. Chlorobenzene-d<sub>5</sub> was chosen to minimize solvent absorption in the wavelength region of interest.

TPA cross-sections were measured using the open aperture Z-scan technique.<sup>49-50</sup> A
Yb:KGW regenerative amplifier (Pharos, Light Conversion) operating at 2 mJ and 10 kHz was used to generate 1030 nm, 170 fs pulses. Approximately 1.3 mJ of this output was directed into

an optical parametric amplifier (OPA, Orpheus-HE, Light Conversion) to generate wavelengths from 0.35 – 16 µm; in this study the idler interaction was used to provide wavelengths from 1400 - 1750 nm. Longpass filters were used to ensure no visible signal leakage was transmitted to the sample. The experimental Z-scan setup is shown in Figure 1S. Briefly, an achromatic halfwaveplate and polarizer pair were used in conjunction with neutral density filters to adjust the pump energy used for the experiment. The beam was then spatially filtered to produce a uniform Gaussian beam by focusing through a diamond pinhole (Fort Wayne Wire Die) and recollimating; an iris diaphragm was placed after this spatial filter and was used to remove any weak diffraction rings still observed. The beam was then split using a wedged reflective neutral density filter; the transmitted portion was used as a reference. The reflected portion was then focused through the sample translation area using a focal length of 150 mm, and the incident beam size on this lens was set using ID2 (Figure 1S) to ensure a free-space Rayleigh range that satisfied the thin sample approximation.<sup>49-50</sup> The beam was then refocused and the signal was measured using a photodetector. A variable neutral density filter was placed in front of both the signal and reference photodetectors so that the signal intensities could be matched. The signal from the photodetectors (PDA50B2 amplified Ge photodetector, Thorlabs) was analyzed using a 50 MHz lock-in amplifier (HF2LI, Zurich Instruments) and custom LabVIEW software that also controlled the sample translation stage (IMS100, Newport).

After spatial filtering, L4 was removed (Figure 1S) and the beam quality was verified using a beam profiling camera. This lens was replaced, and the average power was measured immediately after L4 (well before the focal plane) using an Ophir RM9 pyroelectric sensor/RMC1 chopper. The peak irradiance,  $I_{\theta}$ , was then calculated according to the following equation:

$$I_0 = \frac{2E}{\pi^{3/2} w_0^2 \tau_{HW1/e}} \tag{5}$$

where E is the pulse energy,  $w_0$  is the beam radius at the waist, and  $\tau_{HWI/e}$  is the pulse width (HW1/e). The beam waist and pulse width were determined through a combination of knife-edge measurements and open- and closed-aperture z-scan experiments on the standards GaAs and fused silica, respectively. Solutions of PhC=CPDT-BT and PhC=CPDT-BSe in chlorobenzene- $d_5$  were measured in 1 mm pathlength NIR-grade quartz cuvettes; the response of pure chlorobenzene- $d_5$  was also measured to ensure that there was no contribution to the overall signal from the solvent. The open-aperture z-scan data were then fit according to the methodology of Sheik-Bahae et al.<sup>49-50</sup>

$$T(z, S = 1) = \sum_{m=0}^{\infty} \frac{[-q_0(z, 0)]^m}{(m+1)^{3/2}}$$
 (6)

where z is the sample position, and m is the number of terms in the Gaussian decomposition. The term  $q_0$  is defined as:

$$q_0(z,t) = \frac{\beta I_0(t) \left(\frac{1 - e^{-\alpha L}}{\alpha}\right)}{1 + \frac{z^2}{z_0^2}}$$
 (7)

where  $\beta$  is the two photon absorption coefficient,  $\alpha$  is the linear absorption coefficient, L is the sample pathlength, and  $z_0$  is the Rayleigh length of the beam. After fitting the data for  $\beta$ , the two photon absorption cross-section,  $\delta$ , can be calculated using:<sup>51</sup>

$$\delta = \frac{\beta hc}{N_0 \lambda} \tag{8}$$

where  $\lambda$  is the laser wavelength used, and  $N_{\theta}$  is the sample concentration expressed in units of molecules/cm<sup>3</sup>.

#### III. Results and Discussion

### A. Structures and Relative Energies

For the CPDT-BT and PhC=CPDT-BT monomers, the CPDT and BT units can adopt a *syn* or an *anti*-conformation, where the sulfur atoms in the BT and CPDT rings are located on the same or opposite sides, respectively (Figure 2S). The BT and CPDT rings are coplanar for the CPDT-BT isomers while the PhC=C substitution induces a small twist (~ 15° for the S-C-C-C dihedral angle) between the adjacent donor and acceptor rings. For one monomer unit, the *anti*-conformations are lower in energy compared to the *syn*-conformations by 1-2 kcal/mol. Because of *anti-syn* cumulative effects, we consider the lower energy monomers in oligomer formation. Linear-chain oligomers were generated with the CPDT units with Me or PhC=C substituents pointing in opposite directions, while the corresponding substituents were located on the same side for the curved conformations.

Figure 2 shows the optimized structures for curved and linear conformers of CPDT-BT (a), PhC=CPDT-BT (b), and PhC=CPDT-BSe (c) with n = 10, where n is the number of repeat units. Linear and curved short-chain CPDT-BT oligomers were found to have planar  $C_s$  structures, while the curved structures were lower in energy, consistent with the arched shape reported for the CPDT-BT tetramer. It is important to note that the presence of solubilizing groups that are often necessary for solution processing can affect the conformation of the backbone. The linear-curved (LC) gas-phase energy differences ( $\Delta E_{LC}$ ) was small (less than 1 kcal/mol) for n = 2, increased to about 6 kcal/mol for n = 10, but reduced to about 1-2 kcal/mol in solvents (Table 1S). With enough repeat units, the curved conformer might complete a circular structure through coupling of the end groups, but to avoid steric clashes of the end groups further growth could result in formation of a spiral.

In contrast, PhC=CPDT-BT structures (Figure 3S) and PhC=CPDT-BSe oligomers are distorted in various shapes depending on the rotations of the Ph rings (Figures 4S-6S). For example, parallel (opposite) alignments of Ph rings produced curved-spiral (linear-twisted) structures (Figure 2b). The linear form was previously considered.<sup>6</sup> Notably, despite the large structural changes among isomers with different Ph alignments for a given (curved or linear) motif (Figures 3S-6S), the energy differences were negligible, of 0.0-0.5 kcal/mol. Bulkier substituents on the phenyl or BT rings might stabilize a particular conformer. The linear-curved energy gaps for PhC=CPDT-BT and PhC=CPDT-BSe oligomers are comparable to their CPDT-BT counterparts, with values of ~ 8 and ~ 4 kcal/mol in the gas-phase for the decamers, respectively (Table 1S). The gap reduces to about ~ 2-3 (-0.3-0.1) kcal/mol for the PhC=CPDT-BT(PhC=CPDT-BSe) decamers in solvents.

For the CPDT-BBT and PhC=CPDT-BBT monomers, rotating the C-C single bond connecting the BBT and CPDT groups does not lead to a new isomer. However, the BBT-based copolymers (Figure 3) formed with all Me or PhC=C- groups on the same side resulted in curved conformations similar to the BT-based copolymers discussed above. Interestingly, the linear and curved configurations were found to be isoenergetic for the CPDT-BBT and PhC=CPDT-BBT dimers for both the singlet and triplet states in the gas-phase and in solvents (Table 2S). In the gas-phase, the linear configurations are less 1 kcal/mol lower in energy for the pentamers, which increases to ca. 2-3 kcal/mol for the decamers compared to curved counterparts. Chloroform and chlorobenzene solvents do not have a significant effect on the LC relative energies for the dimer and the pentamer while slightly reducing the LC gaps to about 1 and 2 kcal/mol for the CPDT-BBT and PhC=CPDT-BBT decamers, respectively.

Optimized structures for the curved and linear conformers of CPDT-TQ (a) and PhC=CPDT-

TQ (b) for n = 10 are shown in Figure 4. Linear and curved CPDT-TQ oligomers were found to have planar  $C_s$  structures while PhC=CPDT-TQ counterparts have distorted backbones due to the PhC=C bridgehead substituent. Linear oligomers comprised of the CPDT and TQ units were found to be much higher in energy compared to the curved isomers (Table 4S). The LC gap increases with oligomer length, to about 20 and 18 kcal/mol for the CPDT-TQ and PhC=CPDT-TQ decamers, respectively, in the gas-phase. Solvents reduce  $\Delta E_{LC}$  by about 2-3 kcal/mol.

The curved/spiral oligomers comprised of PhC=CPDT (or CPDT) donors and BT, BSe, and TQ acceptors, were found to be energetically more favorable compared to the corresponding linear isomers and exhibited strong rotational strengths with markedly different ECD spectra compared to the linear structures (Figure 7S). The ECD spectra for the PhC=CPDT-BT, PhC=CPDT-BSe, and PhC=CPDT-TQ spiral structures are shown in Figure 5. For PhC=CPDT-BT (PhC=CPDT-BSe), two ECD bands occur at 1.22 and 1.84 eV (1.24 and 1.76 eV), a red-shift of about 0.3 eV (0.2 eV) compared to the first linear absorption peak. A similar red-shift (0.2 eV) from the first linear absorption peak is obtained for the first ECD band (0.51 eV) for the PhC=CPDT-TQ decamer; the intensity of the second band at 1.23 eV is weak.

## **B.** Singlet-Triplet Gaps

Table 1 summarizes our calculated B3LYP singlet-triplet gaps ( $\Delta E_{\rm ST} = E_{\rm S} - E_{\rm T}$ ) and available experimental values. Figure 6 shows the computed  $\Delta E_{\rm ST}$  in the gas-phase. CPDT-BT oligomers are predicted to have a closed shell singlet ground state, with  $\Delta E_{\rm ST}$  in the range of -18 to -19 kcal/mol for oligomers with n=10. The gaps are not significantly different for the pentamer and increased by about 3 kcal/mol for the dimer. The  $\Delta E_{\rm ST}$  gaps of about -31 and -32 kcal/mol obtained for the PhC=CPDT-BT and CPDT-BT monomers, respectively, as well as those for the

dimers and pentamers, were reduced by 2-3 kcal/mol for n = 1, 2, and 5 after including zeropoint energy corrections (Table 1).

The PhC=CPDT-BBT and CPDT-BBT monomers and dimers exhibit a singlet ground state with classical  $\Delta E_{\rm ST} \sim -10$  and -2 kcal/mol, respectively (Table 1, Figure 6). The singlet and triplet states are degenerate for n=5, which is shorter in oligomer length compared other DA oligomers. Singlet-triplet gaps for the linear PhC=CPDT-BBT oligomers that were previously reported<sup>17</sup> <sup>19</sup> are similar to the values obtained in this work. Experimentally,  $\Delta E_{\rm ST}$  of 8.73  $\times$  10<sup>-3</sup> kcal/mol was obtained from EPR data for PhC=CPDT-BBT with -C<sub>16</sub>H<sub>33</sub> side chains.<sup>17</sup>

The singlet and triplet states for the PhC=CPDT-TQ linear and curved oligomers (n = 10) are predicted to be isoenergetic (Table 1, Figure 6). For the alkyl-bridging CPDT-TQ decamer, the computed  $\Delta E_{\rm ST}$  values are in the range of 0.0 to -0.3 kcal/mol. The reported  $\Delta E_{\rm ST}$  values for the linear models of PhC=CPDT-TQ<sup>6</sup> and CPDT-TQ<sup>18</sup> are -0.6 and -0.4 kcal/mol, respectively, for n = 8. Singlet ground states are predicted for the shorter pentamer oligomers and dimers of PhC=CPDT-TQ and CPDT-TQ, with  $\Delta E_{\rm ST}$  gaps of 1-2 kcal/mol for n = 5 and 8-9 kcal/mol for n = 2 (Table 1). Synthesized copolymers comprised of the CPDT donors with the hexadecyl (-C<sub>16</sub>H<sub>33</sub>)<sup>18</sup> and 3,5-didodecylbenzylidene (PhC=CPDT,  $R = -C_{12}H_{25}$ )<sup>6</sup> bridging groups and the TQ acceptor were reported to have a triplet ground states through EPR spectroscopy, where  $\Delta E_{\rm ST} = 7.81 \times 10^{-3}$  kcal/mol<sup>7</sup> and  $\Delta E_{\rm ST} = 9.30 \times 10^{-3}$  kcal/mol, respectively.<sup>6</sup>

# C. Absorption Spectra

We first discuss the performance of different functionals using TD-DFT, TDA, and sTDA, and then compare the computed spectra to corresponding experimental data for each system.

Table 2 summarizes the TD-B3LYP and TDA-(OT-CAMB3LYP) results and available

experimental first OPA maxima ( $\lambda_{Max}$ ) for the six oligomers. The computed results (summarized in Table 4S for a range of functionals) were obtained using the decamer structures. The results agree with experiment, but systematically underestimate the experimental values by 0.24 eV using TD-B3LYP. TDA-B3LYP slightly improves the results with a mean error (ME) and mean absolute error (MAE) of -0.19 and 0.19 eV, respectively. Applying the TDA-PBE0 method further reduces the MAE to 0.13 eV (ME = -0.10 eV), but sTDA increases the MAEs to 0.30 and 0.34 eV when using the PBE0 and B3LYP functionals, respectively. sTDA-CAMB3LYP overestimates  $\lambda_{Max}$  by an average of 0.33 eV. Notably, using TDA-OT-CAMB3LYP results in the lowest MAE of 0.09 eV (ME = -0.04). The MAE (0.13 eV) and ME (-0.08 eV) are not significantly changed using PCM-TDA-OT-CAMB3LYP to account for solvent effects. Thus, although using the TDA method with the B3LYP or PBE0 hybrid functionals provided reasonable results, employing TDA-OT-CAMB3LYP resulted in an overall improved prediction of  $\lambda_{Max}$  (Figure 7), and thus will be primarily used for the description of excited states for the polymers considered.

We begin by discussing the OPA spectra for CPDT-BT oligomers. The first experimental absorption peaks in o-dichlorobenzene at room temperature for  $R = C_{12}H_{25}$  and R = 2-ethylhexyl were reported to occur at 1.55 and 1.68 eV, respectively.<sup>55</sup> However, nearly identical absorption spectra were observed for the two alkyl groups at elevated temperatures, which presumably break up interchain aggregates. This is consistent with the spectral maximum of 1.73 eV in Figure 7, as reported for the long alkyl chains ( $R = C_{16}H_{33}$ ) that inhibit  $\pi$ -stacking.<sup>56</sup> For the CPDT-BT decamer, TDA underestimates (overestimates) the first transition maximum by 0.16 (0.24) and 0.34 (0.04) eV using the OT-CAMB3LYP and the PBE0 functionals, respectively. The two lowest strong transitions, originating primarily from the HOMO to LUMO and HOMO

1 to the LUMO (Figure 8S) are predicted to represent major contributions to the first absorption band. Electrons in the HOMO and HOMO − 1 are delocalized over almost the entire chain length with some charge depletion in the periphery (central) region for the HOMO (HOMO − 1). The LUMO is also delocalized with increasing participation from the BT units.
 Thus, the first two transitions do have some CT character, which is more appropriately described by the long-range corrected functionals.

Experimentally, replacing the bridging alkyls in CPDT units with PhC=C groups ( $R = C_{12}H_{25}$ for solubility) produces a broad first absorption band that extends the band edge to the SWIR.<sup>48</sup> The  $\lambda_{\text{Max}}$  in chloroform (Figure 7) and  $S_1$  (estimated from the absorption onset of a thin film) decrease to 1.53 and ~ 1.1 eV, respectively. 48 The absorption is predicted by TDA-OT-CAMB3LYP to occur at about the same  $\lambda_{Max}$  value (1.55 eV), while the corresponding  $S_1$  (1.46 eV) is overestimated due to the effects of  $\pi$ -stacking in thin films. Compared to the alkyl substituted CPDT-BT, small red-shifts are observed for  $\lambda_{\text{Max}}$  (0.20 eV) and S<sub>1</sub> (0.14 eV), which might be attributed to the effects of different solvents and/or side chains. Replacing the BTs with benzoselenadiazole (BSe) acceptors resulted in a small red-shift of absorption band to 1.47 eV using TDA-OT-CAMB3LYP calculations, in good agreement with the measured value of 1.41 eV. Note that Boltzmann averaging for three curved/spiral structures does not change the  $\lambda_{\text{Max}}$  values for PhC=CPDT-BT and PhC=CPDT-BSe. The S<sub>1</sub> (1.08 eV) transition energy, estimated from the absorption onset of the thin film, is similarly lower compared to the TDA-OT-CAMB3LYP predicted value of 1.39 eV. Similar to the CPDT-BT decamer, the two lowest transitions S<sub>1</sub> and S<sub>2</sub> involve predominantly HOMO to LUMO and HOMO – 1 to LUMO excitations, respectively. These are predicted to underlie the first absorption band for the PhC=CPDT-BSe and PhC=CPDT-BT decamers. The MOs for PhC=CPDT-BT and

PhC=CPDT-BSe decamers (Figures 9S and 10S) are delocalized over the nonplanar backbones. As PhC=C groups are not strongly coupled to the backbones, these MOs, therefore, show a similar degree of delocalization compared to the corresponding MOs for the CPDT-BT decamer.

Long-chain oligomers with PhC=CPDT donors and BBT acceptors, which were predicted<sup>19</sup> to have near zero  $\Delta E_{\rm ST}$ , have been synthesized and characterized recently.<sup>17</sup> The absorption spectrum of PhC=CPDT-BBT ( $R = C_{16}H_{33}$ ) has a broad band that extends to the mid-infrared region, with an estimate optical gap of 0.28 eV for a thin film and  $\lambda_{Max}$  of 1.01 eV in chlorobenzene. The TDA predicted absorption maxima for PhC=CPDT-BBT and CPDT-BBT oligomers are within 0.1 eV of experiment for the functionals OT-CAMB3LYP, B3LYP, and PBE0. For OT-CAMB3LYP, the first 25 excited states within the 0.7-1.5 eV energy range are predicted to contribute the first broad absorption band (Figure 11S). The large number of excited states within a small energy range can be attributed to MOs that are closely spaced in energy with two nearly degenerate singly occupied MOs (Figures 12S and 13S). The most intense transition ( $T_1 \rightarrow T_{11}$ ), located at 1.06 eV (f = 13.75), has major excitations from HOMO, HOMO -2, and HOMO -1 to LUMO, LUMO +1, and LUMO +2 ( $\alpha$ -HOMO  $-1 \rightarrow \alpha$ -LUMO,  $\alpha$ - $HOMO - 1 \rightarrow \alpha$ -LUMO + 1,  $\beta$ -HOMO - 1  $\rightarrow \beta$ -LUMO + 1,  $\beta$ -HOMO - 1  $\rightarrow \beta$ -LUMO + 2). Excitations from the spatially separated unpaired electrons to the LUMO and higher-energy virtual orbitals have CT-like character. However, there is significant overlap between the electrons and holes, leading to large oscillator strengths.

Natural transition orbitals (NTOs) that are obtained through unitary transformation of the transition density matrix often reduce the mixed transitions involved in multiple one-electron excitations to a single (or a small number) pair of holes in the occupied space, and electrons (excited to virtual space) with an associated eigenvalue  $\lambda$  (contributing weight).<sup>57</sup> Interestingly,

the NTOs representing the major contributions of one-electron excitations do not offer a simplified description for the  $T_1 \rightarrow T_{11}$  transition (Figure 14S), as the dominant contributing weights are small,  $\lambda = 0.28$  and 0.26 for the  $\alpha$ -NTO and  $\beta$ -NTO pairs, respectively. Compared to PhC=CPDT-BT, the large red-shift (0.4 eV) induced by the BBT groups can be attributed to the larger and smaller stabilization of the virtual and occupied MOs, respectively (cf. Figures 9S, 12S, and 13S). The optical gap is comprised of three nearly degenerate transitions is predicted to be  $\sim 0.7$  eV, much larger than the experimental value obtained from thin films of PhC=CPDT-BBT (R =  $C_{16}H_{33}$ ).

Donor-acceptor conjugated polymers comprised of TQ and CPDT with -C<sub>16</sub>H<sub>33</sub> and the PhC=C ( $R = C_{12}H_{25}$ ) groups have been reported to have open-shell high-spin ground states and low absorption peaks/maxima? at 0.82 and 0.99 eV, respectively. 6-7, 18 TDA maxima with similar  $\lambda_{Max}$  values (0.8 – 0.9 eV) were calculated for the CPDT-TDQ and PhC=CPDT-TDQ decamers. A large number of excited states contributed to the first absorption bands (Figure 15S), similar to the results obtained for the PhC=CPDT-BBT and CPDT-BBT oligomers. The most intense transitions ( $T_1 \rightarrow T_5$ , 0.68 eV, f = 5.83 for PhC=CPDT-TDQ; 0.69 eV, f = 7.30 for CPDT-TQ) involve predominantly HOMO  $\rightarrow$  LUMO and HOMO  $-1 \rightarrow$  LUMO + 1 transitions for the  $\alpha$ - and  $\beta$ -orbitals (Figures 16S-19S). Two ( $\alpha$  and  $\beta$ ) sets of NTOs account for the major contribution to the  $T_1 \rightarrow T_5$  transitions for CPDT-TQ decamer (Figures 20S) and PhC=CPDT-TQ (Figures 21S), which reveal CT character attributed to the β-NTOs. The holes and electrons α-NTOs are more delocalized. Compared to the alkyl-substituted CPDT-TQ, an uncharacteristic observed blue shift of 0.17 eV exerted by the PhC=C ( $R = C_{12}H_{25}$ ) groups is not reproduced by the computed results, which could be attributed to aggregation or more extended conjugation.<sup>7</sup>

The computed TPA spectra for the PhC=CPDT-BT and PhC=CPDT-BSe decamers are shown in Figure 8, using the B3LYP and PBE0 hybrid functionals, and the OT-CAMB3LYP functional. For the PhC=CPDT-BT (PhC=CPDT-BSe) decamer, the first TPA maxima were found to occur at slightly ( $\sim 0.3$  eV) higher energy relative to the first OPA maxima, of  $\sim 1.6$ (1.5) and 1.8 (1.7) eV for the B3LYP and PBE0 functionals, respectively. The predicted values are consistent with experimental TPA maxima at about 1.6 eV (Figure 22S). However, the predicted cross-sections (~ 10<sup>5</sup> GM for the B3LYP and PBE0 functionals) severely overestimate the experimental TPA maxima in the range of 1500–3500 GM for PhC=CPDT-BT ( $R = C_{12}H_{25}$ ) and 1000–3000 GM for PhC=CPDT-BSe ( $R = C_{12}H_{25}$ ). Employing the sTD/B3LYP and sTD/PBE0 methods decreases the magnitude of the cross-sections by more than a factor of two as compared to the corresponding TD and TDA values. The sTD-OT-CAMB3LYP crosssections are small below 2 eV (as calculated by including the first 9 excited states) but are very large ( $\sim 10^5$  GM) at higher energy. The first TPA maximum cross-section of about 130 GM ( $\sim$ 1.8 eV) and 260 GM (~ 1.6 eV) were obtained for the PhC=CPDT-BT and the PhC=CPDT-BSe decamers, respectively. These values are consistent with the TDA-OT-CAMB3LYP crosssections of about 260 GM (~ 1.9 eV) and 490 GM (~ 1.8 eV) obtained below 2 eV for the PhC=CPDT-BT and PhC=CPDT-BSe decamers, respectively. Our results confirm recent TPA benchmarking for 48 donor-acceptor molecules, 58 where underestimation of the TPA crosssections were attributed to an underestimation of the excited state dipole moment<sup>58</sup> that can be obtained by quadratic response TD-DFT<sup>46</sup> and its simplified form,<sup>37</sup> which will be addressed in future work.

#### IV. Conclusions

We report on structures, relative energies, singlet-triplet gaps, and absorption spectra for longchain DACOs comprised of substituted CPDT donors with benzothiadiazole, benzoselenadiazole, benzobisthiadiazole, and thiadiazologuinoxaline acceptors, having up to ten repeating units. Linear oligomers were found to be energetically less favorable compared to the curved/spiral isomers. In contrast, oligomers with benzobisthiadiazole prefer linear geometry. Oligomers with benzobisthiadiazole and thiadiazoloquinoxaline acceptors have narrow singlet-triplet gaps that become degenerate for long-chain oligomers. Based on the computed DFT decamer structures, we found good agreement between observed and calculated first absorption maxima, with MAEs of 0.24 and 0.20 eV using TD-DFT and TDA, respectively, using the B3LYP functional. The TDA errors are reduced using the PBE0 (MAE = 0.13 eV) and optically tuned OT-CAMB3LYP (MAE  $\sim 0.1$  eV) functionals, but the efficient simplified TDA (sTDA) method for treating large systems increases the MAEs to 0.30 and 0.34 eV using the PBE0 and B3LYP functionals, respectively. Our computed TPA spectra for the PhC=CPDT-BT and PhC=CPDT-BSe decamers are consistent with our measured experimental TPA maxima at about 1.6 eV, yet the cross-sections are overestimated employing the B3LYP and PBE0 functionals but underestimated by OT-CAMB3LYP. Limitations in predicting cross-sections by RSH functionals for donor-acceptor molecules has been recently pointed out in a benchmarking study, where hybrid functionals were shown to provide improved agreement compared to the single-reference CC2 method.<sup>58</sup> The overestimation of the cross-section in comparison to experiment for the DACOs studied here could potentially be attributed also to effects of concentration.

# Acknowledgements

We gratefully acknowledge support provided by the Air Force Office of Scientific Research

(AFOSR) the Molecular Dynamics and Theoretical Chemistry Program (Program Manager: Dr. Michael R. Berman) and computational resources and helpful assistance provided by the Air Force Research Laboratory (AFRL) DoD Supercomputing Resource Center. L.M.L. acknowledges funding under AFRL/RXEP contract FA8650-22-D-5408. The work performed at The Georgia Institute of Technology was made possible by the National Science Foundation (NSF) award DMR-2323665 and AFOSR support provided by the Organic Materials Chemistry Program (Grant FA9550-23-1-0654, Program Manager: Dr. Kenneth Caster).

## **Supporting Information Available**

B3LYP-D3/6-31G(d,p) linear relative energies compared to the curved conformers for: CPDT-BT, PhC=CPDT-BT, PhC=CPDT-BSe, PhC=CPDT-BBT, CPDT-BBT, and PhC=CPDT-TQ, and CPDT-TQ. OPA maxima, extinction coefficients, and first transition energies. Singlet B3LYP/6-31G(d,p) for structures and relative energies for CPDT-BT, PhC=CPDT-BT, CPDT-TQ, and PhC=CPDT-TQ monomers. TDA-B3LYP ECD spectra for the spiral and linear conformers of PhC=CPDT-BT decamer. Detailed MO analyses. Measured TPA degenerate Z-scan for the PhC=CPDT-BT and PhC=CPDT-BSe decamers. This material is available free of charge via the Internet at http://pubs.acs.org.

# References

- 1. Müllen, K.; Scherf, U., Conjugated Polymers: Where We Come From, Where We Stand, and Where We Might Go. *Macromolecular Chemistry and Physics* **2023**, *224* (3), 2200337.
- 2. Qiu, Z.; Hammer, B. A.; Müllen, K., Conjugated polymers—Problems and promises. *Progress in Polymer Science* **2020**, *100*, 101179.
- 3. R. Murad, A.; Iraqi, A.; Aziz, S. B.; N. Abdullah, S.; Brza, M. A., Conducting polymers for optoelectronic devices and organic solar cells: A review. *Polymers* **2020**, *12* (11), 2627.
- 4. Huang, Y.; Egap, E., Open-shell organic semiconductors: an emerging class of materials with novel properties. *Polymer Journal* **2018**, *50* (8), 603-614.
- 5. Chen, Z.; Li, W.; Sabuj, M. A.; Li, Y.; Zhu, W.; Zeng, M.; Sarap, C. S.; Huda, M. M.; Qiao, X.; Peng, X., Evolution of the electronic structure in open-shell donor-acceptor organic semiconductors. *Nature Communications* **2021**, *12* (1), 5889.

- 6. London, A. E.; Chen, H.; Sabuj, M.; Tropp, J.; Saghayezhian, M.; Eedugurala, N.; Zhang, B.; Liu, Y.; Gu, X.; Wong, B., A high-spin ground-state donor-acceptor conjugated polymer. *Science advances* **2019**, *5* (5), eaav2336.
- 7. Huang, L.; Eedugurala, N.; Benasco, A.; Zhang, S.; Mayer, K. S.; Adams, D. J.; Fowler, B.; Lockart, M. M.; Saghayezhian, M.; Tahir, H., Open-Shell Donor–Acceptor Conjugated Polymers with High Electrical Conductivity. *Advanced Functional Materials* **2020**, *30* (24), 1909805.
- 8. Nakano, M., Open-Shell-Character-Based Molecular Design Principles: Applications to Nonlinear Optics and Singlet Fission. *The Chemical Record* **2017**, *17* (1), 27-62.
- 9. Huang, Y.-Q.; Jiang, S.-S.; Pan, L.-X.; Zhang, R.; Liu, K.-L.; Liu, X.-F.; Fan, Q.-L.; Wang, L.-H.; Huang, W., A zwitterionic red-emitting water-soluble conjugated polymer with high resistance to nonspecific binding for two-photon cell imaging and good singlet oxygen production capability. *New J. Chem.* **2021**, *45* (34), 15607-15617.
- 10. Shen, X.; Li, L.; Min Chan, A. C.; Gao, N.; Yao, S. Q.; Xu, Q.-H., Water-Soluble Conjugated Polymers for Simultaneous Two-Photon Cell Imaging and Two-Photon Photodynamic Therapy. *Adv. Opt. Mater.* **2013**, *1* (1), 92-99.
- 11. Rodríguez-Rea, J.; Güizado-Rodríguez, M.; Maldonado, J.-L.; Ramos-Ortiz, G.; Reveles, J. U.; Silva, C.; Barba, V.; Saucedo-Salazar, E. M.; Rodríguez Hernández, M. T., Synthesis of Donor-Acceptor Copolymers Derived from Diketopyrrolopyrrole and Fluorene via Eco-Friendly Direct Arylation: Nonlinear Optical Properties, Transient Absorption Spectroscopy, and Theoretical Modeling. *Energies* **2022**, *15* (11).
- 12. Blacha-Grzechnik, A., New Approach in the Application of Conjugated Polymers: The Light-Activated Source of Versatile Singlet Oxygen Molecule. *Materials* **2021**, *14* (5), 1098.
- 13. Ramasundaram, S.; Sobha, S.; Saravanakumar, G.; Oh, T. H., Recent Advances in Biomedical Applications of Polymeric Nanoplatform Assisted with Two-Photon Absorption Process. *Polymers* **2022**, *14* (23).
- 14. Li, N.; Mahalingavelar, P.; Vella, J. H.; Leem, D.-S.; Azoulay, J. D.; Ng, T. N., Solution-processable infrared photodetectors: Materials, device physics, and applications. *Mater. Sci. Eng., R* **2021**, *146*, 100643.
- 15. Solak, E. K.; Irmak, E., Advances in organic photovoltaic cells: a comprehensive review of materials, technologies, and performance. *RSC Advances* **2023**, *13* (18), 12244-12269.
- 16. Bei, Q.; Zhang, B.; Wang, K.; Zhang, S.; Xing, G.; Cabanetos, C., Benzothiadiazole-based materials for organic solar cells. *Chin. Chem. Lett.* **2023**, 108438.
- 17. Steelman, M. E.; Adams, D. J.; Mayer, K. S.; Mahalingavelar, P.; Liu, C.-T.; Eedugurala, N.; Lockart, M.; Wang, Y.; Gu, X.; Bowman, M. K.; Azoulay, J. D., Magnetic Ordering in a High-Spin Donor–Acceptor Conjugated Polymer. *Adv. Mater.* **2022**, *34* (45), 2206161.
- 18. Joo, Y.; Huang, L.; Eedugurala, N.; London, A. E.; Kumar, A.; Wong, B. M.; Boudouris, B. W.; Azoulay, J. D., Thermoelectric Performance of an Open-Shell Donor–Acceptor Conjugated Polymer Doped with a Radical-Containing Small Molecule. *Macromolecules* **2018**, *51* (10), 3886-3894.
- 19. Sabuj, M. A.; Huda, M. M.; Sarap, C. S.; Rai, N., Benzobisthiadiazole-based high-spin donor—acceptor conjugated polymers with localized spin distribution. *Mater. Adv.* **2021**, *2* (9), 2943-2955.

- 20. Ku, J.; Gim, Y.; Lansac, Y.; Jang, Y. H., N-Alkylthienopyrroledione versus benzothiadiazole pulling units in push–pull copolymers used for photovoltaic applications: density functional theory study. *Phys. Chem. Chem. Phys.* **2016**, *18* (2), 1017-1024.
- 21. Turan, H. T.; Kucur, O.; Kahraman, B.; Salman, S.; Aviyente, V., Design of donor–acceptor copolymers for organic photovoltaic materials: a computational study. *Phys. Chem. Chem. Phys.* **2018**, *20* (5), 3581-3591.
- 22. Stratmann, R. E.; Scuseria, G. E.; Frisch, M. J., An efficient implementation of time-dependent density-functional theory for the calculation of excitation energies of large molecules. *J. Chem. Phys.* **1998**, *109*, 8218.
- 23. Hirata, S.; Head-Gordon, M., Time-dependent density functional theory within the Tamm-Dancoff approximation. *Chem. Phys. Lett.* **1999**, *314*, 291.
- 24. Grimme, S., A simplified Tamm-Dancoff density functional approach for the electronic excitation spectra of very large molecules. *J. Chem. Phys.* **2013**, *138* (24), 244104.
- 25. Kohn, W.; Sham, L. J., Self-consistent field equations including exchange and correlation effects. *Phys. Rev.* **1965**, *140*, A1133–A1138.
- 26. Becke, A. D., Density-functional exchange-energy approximation with correct asymptotic behavior. *Phys. Rev. A* **1988**, *38*, 3098.
- 27. Lee, C.; Yang, W.; Parr, R. G., Development of the Colle-Salvatti correlation-energy formula into a functional of the electron density. *Phys. Rev. B* **1988**, *37*, 785.
- 28. Becke, A. D., Density-functional thermochemistry. III. The role of exact exchange. *J. Chem. Phys.* **1993**, *98*, 5648.
- 29. Grimme, S.; Antony, J.; Ehrlich, S.; Krieg, H., A consistent and accurate ab initio parametrization of density functional dispersion correction (DFT-D) for the 94 elementsH-Pu. *J. Chem. Phys.* **2010**, *132*, 154104.
- 30. Hehre, W. J.; Ditchfield, R.; Pople, J. A., Self—Consistent Molecular Orbital Methods. XII. Further Extensions of Gaussian—Type Basis Sets for Use in Molecular Orbital Studies of Organic Molecules. *J. Chem. Phys.* **1972**, *56*, 2257–2261.
- 31. Francl, M. M.; Pietro, W. J.; Hehre, W. J.; Binkley, J. S.; DeFrees, D. J.; Pople, J. A.; Gordon, M. S., Self-Consistent Molecular Orbital Methods. 23. A Polarization-Type Basis Set for 2nd-Row Elements. *J. Chem. Phys.* **1982**, *77*, 3654–3665.
- 32. Bergner, A.; Dolg, M.; Kuechle, W.; Stoll, H.; Preuss, H., Ab-initio energy-adjusted pseudopotentials for elements of groups 13-17. *Mol. Phys.* **1993**, *80*, 1431–1441.
- 33. Martin, J. M. L.; Sundermann, A., Correlation consistent valence basis sets for use with the Stuttgart-Dresden-Bonn relativistic effective core potentials: The atoms Ga Kr and In Xe *J. Chem. Phys.* **2001**, *114*, 3408.
- 34. Frisch, M. J.; Trucks, G. W.; Schlegel, H. B.; Scuseria, G. E.; Robb, M. A.; Cheeseman, J. R.; Scalmani, G.; Barone, V.; Mennucci, B.; Petersson, G. A.; Nakatsuji, H., et al. *Gaussian 16, Revision C.01*, C.01; Gaussian, Inc.: Wallingford CT, 2016.
- 35. Bauernschmitt, R.; Häser, M.; Treutler, O.; Ahlrichs, R., Calculation of excitation energies within time-dependent density functional theory using auxiliary basis set expansions. *Chem. Phys. Lett.* **1997**, *264* (6), 573-578.
- Balasubramani, S. G.; Chen, G. P.; Coriani, S.; Diedenhofen, M.; Frank, M. S.; Franzke, Y. J.; Furche, F.; Grotjahn, R.; Harding, M. E.; Hättig, C.; Hellweg, A.; Helmich-Paris, B.; Holzer, C.; Huniar, U.; Kaupp, M.; Marefat Khah, A.; Karbalaei Khani, S.; Müller, T.; Mack, F.; Nguyen, B. D.;

- Parker, S. M.; Perlt, E.; Rappoport, D.; Reiter, K.; Roy, S.; Rückert, M.; Schmitz, G.; Sierka, M.; Tapavicza, E.; Tew, D. P.; van Wüllen, C.; Voora, V. K.; Weigend, F.; Wodyński, A.; Yu, J. M., TURBOMOLE: Modular program suite for ab initio quantum-chemical and condensed-matter simulations. *J. Chem. Phys.* **2020**, *152* (18), 184107.
- 37. de Wergifosse, M.; Grimme, S., Nonlinear-response properties in a simplified time-dependent density functional theory (sTD-DFT) framework: Evaluation of the first hyperpolarizability. *J. Chem. Phys.* **2018**, *149* (2), 024108.
- 38. Grimme, S.; de Wergifossea, M. *sTDA*, 1.6.2; 2020.
- 39. Adamo, C.; Barone, V., Toward Reliable Density Functional Methods without Adjustable Parameters: The PBE0 Model. *J. Chem. Phys.* **1999**, *110*, 6158–6170.
- 40. Stein, T.; Kronik, L.; Baer, R., Reliable prediction of charge transfer excitation in molcular complexes using time-dependent density functional theory. *J. Am. Chem. Soc* **2009**, *131*, 2818.
- 41. Nguyen, K. A.; Day, P. N.; Pachter, R., The performance and relationship among range-separated schemes for density functional theory. *J. Chem. Phys.* **2011**, *135*, 074109/1–074109/10.
- 42. Körzdörfer, T.; Brédas, J.-L., Organic Electronic Materials: Recent Advances in the DFT Description of the Ground and Excited States Using Tuned Range-Separated Hybrid Functionals. *Acc. Chemi. Res.* **2014**, *47* (11), 3284-3291.
- 43. Yanai, T.; Tew, D. P.; Handy, N. C., A New Hydrid Exchange-Correlation Functional using the Coulomb-Attenuating Method (CAM-B3LYP). *Chem. Phys. Lett.* **2004**, *393*, 51–57.
- 44. Nguyen, K. A.; Day, P. N.; Pachter, R., One- and Two-photon Spectra of Platinum Acetylide Chromophores: A TDDFT Study. *J. Phys. Chem. A* **2009**, *113*, 13943–13952.
- 45. Stephens, P. J.; Harada, N., ECD cotton effect approximated by the Gaussian curve and other methods. *Chirality* **2010**, *22* (2), 229-233.
- 46. Parker, S. M.; Rappoport, D.; Furche, F., Quadratic Response Properties from TDDFT: Trials and Tribulations. *J. Chem. Theory Comput.* **2018**, *14* (2), 807-819.
- 47. Goppert-Mayer, M., Elementary Acts with Two Quantum Jumps. *Ann. Phys.* **1931**, *401*, 273–294.
- 48. London, A. E.; Huang, L.; Zhang, B. A.; Oviedo, M. B.; Tropp, J.; Yao, W.; Wu, Z.; Wong, B. M.; Ng, T. N.; Azoulay, J. D., Donor–acceptor polymers with tunable infrared photoresponse. *Polym. Chem.* **2017**, *8* (19), 2922-2930.
- 49. Sheik-Bahae, M.; Said, A. A.; Wei, T.-H.; Hagan, D. J.; Van Stryland, E. W., Sensitive measurement of optical nonlinearities using a single beam. *IEEE journal of quantum electronics* **1990**, *26* (4), 760-769.
- 50. Van Stryland, E. W.; Sheik-Bahae, M.; Kuzyk, M.; Dirk, C., Characterization techniques and tabulations for organic nonlinear materials. *MG Kuzyk and CW Dirk, Eds* **1998**, 655-692.
- 51. Rumi, M.; Perry, J. W., Two-photon absorption: an overview of measurements and principles. *Advances in Optics and Photonics* **2010**, *2* (4), 451-518.
- 52. Risko, C.; McGehee, M. D.; Brédas, J.-L., A quantum-chemical perspective into low optical-gap polymers for highly-efficient organic solar cells. *Chem. Sci.* **2011**, *2* (7), 1200-1218.
- 53. Tsao, H. N.; Cho, D. M.; Park, I.; Hansen, M. R.; Mavrinskiy, A.; Yoon, D. Y.; Graf, R.; Pisula, W.; Spiess, H. W.; Müllen, K., Ultrahigh mobility in polymer field-effect transistors by design. *Journal of the American Chemical Society* **2011**, *133* (8), 2605-2612.

- 54. Pisula, W.; Tsao, H. N.; Dudenko, D.; Cho, D. M.; Puniredd, S. R.; Zhao, Y.; Mavrinskiy, A.; Shu, J.; Hansen, M. R.; Baumgarten, M., Solid-state organization and ambipolar field-effect transistors of benzothiadiazole-cyclopentadithiophene copolymer with long branched alkyl side chains. *Polymers* **2013**, *5* (2), 833-846.
- 55. Coffin, R. C.; Peet, J.; Rogers, J.; Bazan, G. C., Streamlined microwave-assisted preparation of narrow-bandgap conjugated polymers for high-performance bulk heterojunction solar cells. *Nat. Chem.* **2009**, *1* (8), 657-661.
- 56. Zhang, M.; Tsao, H. N.; Pisula, W.; Yang, C.; Mishra, A. K.; Müllen, K., Field-Effect Transistors Based on a Benzothiadiazole–Cyclopentadithiophene Copolymer. *J. Am. Chem. Soc.* **2007**, *129* (12), 3472-3473.
- 57. Martin, R. L., Natural transition orbital. J. Chem. Phys. 2003, 118, 4775.
- 58. Chołuj, M.; Alam, M. M.; Beerepoot, M. T. P.; Sitkiewicz, S. P.; Matito, E.; Ruud, K.; Zaleśny, R., Choosing Bad versus Worse: Predictions of Two-Photon-Absorption Strengths Based on Popular Density Functional Approximations. *J. Chem. Theory Comput.* **2022**, *18* (2), 1046-1060.

Table 1. B3LYP-D3/6-31G(d,p) adiabatic singlet-triplet (S-T) gaps ( $E_S - E_T$ , in kcal/mol). Values in parentheses include zero-point energy corrections.

PhC=CPDT-BT			
Isomer/Solvent	Dimer	Pentamer	Decamer
Curveda			
none	-21.4 (-19.5)	-18.6 (-15.8)	-18.5
chloroform	-21.6	-19.0	-19.0
chlorobenzene	-21.6	-19.1	-19.0
Linear			Twisted
none	-20.8 (-18.9)	-17.8 (-15.3)	-17.6
chloroform	-20.8	-18.0	-17.8
chlorobenzene	-20.8	-18.0	-17.8
CPDT-BT			
Curved <sup>a</sup>			
none	-20.9 (-19.2)	-18.7 (-16.3)	-19.4
chloroform	-21.5	-18.7	-19.5
chlorobenzene	-21.5	-18.7	-19.5
Linear			
none	-22.0 (-20.2)	-17.7 (-15.5)	-17.9
chloroform	-20.8	-17.6	-17.8
chlorobenzene	-20.7	-17.6	-17.8
PhC=CPDT-BBT			
Curved			
none	-1.8 (-1.9)	0.0 (-0.1)	-0.4
chloroform	-1.9	0.0	-0.4
chlorobenzene	-1.9	0.0	-0.4
Linear <sup>a</sup>			Bent
none	-1.8 (-1.9)	0.0 (-0.1)	0.0
chloroform	-1.9	0.0	0.0
chlorobenzene	-1.9	0.0	0.0
CPDT-BBT			
Curved			
none	-1.8 (-1.9)	0.0 (0.0)	0.0
chloroform	-1.7	0.0	0.0
chlorobenzene	-1.7	0.0	0.0
Lineara			
none	-1.8 (-1.8)	0.0 (0.0)	0.1
chloroform	-1.7	0.0	-0.2
PhC=CPDT-TQ			
Curved <sup>a</sup> (nonplanar)			
none	-8.0 (-6.6)	-1.5 (-1.6)	0.0
chloroform	-8.8	-2.1	0.0

chlorobenzene	-8.8	-2.1	0.0
o-dichlorobenzene	-9.0	-2.3	0.0
Linear (nonplanar)			
none	-7.9 (-6.5)	-1.4 (-1.6)	0.0
chloroform	-8.6	-1.9	0.0
chlorobenzene	-8.7	-1.9	0.0
o-dichlorobenzene	-8.8	-2.0	0.0
CPDT-TQ			
Curved <sup>a</sup>			
none	-7.8 (-6.5)	-1.2 (-1.5)	0.0
chloroform	-8.3	-1.6	-0.3
chlorobenzene	-8.4	-1.6	-0.3
o-dichlorobenzene	-8.5	-1.7	-0.3
Linear			
none	-7.7 (-6.4)	-1.2 (-1.4)	-0.2
chloroform	-8.2	-1.4	-0.3
chlorobenzene	-8.2	-1.5	-0.3
o-dichlorobenzene	-8.3	-1.5	-0.3

<sup>a</sup>Lower energy structure. Monomer singlet-triplet gaps in the gas phase, chloroform, chlorobenzene: -31.0 (-27.9), -31.1, -31.1 (PhC=CPDT-BT), -31.9 (-30.0), -31.0, -31.0 (CPDT-BT), -9.5 (-8.6), -9.3, -9.3 (PhC=CPDT-BBT), -9.5 (-8.7), -9.2, -9.2 (CPDT-BBT), -18.0 (-16.6), -18.0, -18.0 (Ph=CPDT-MeTDQ), -18.2 (-16.8), -18.2, -18.2 (CPDT-TQ), 16.5 (gas-phase singlet-triplet gap for the PhC=CPDT-BSe decamer).

UB3LYP/6-31G(d,p) singlet-triplet gaps reported by Sabuj et al. <sup>19</sup> for the linear oligomers of Ph=CPDT-BBT: 2.1 (dimer), 0.1 (tetramer), 0.0 (hexamer, octamer). Experimental singlet-triplet gaps:  $8.73 \times 10^{-3}$  kcal/mol for PhC=CPDT-BBT polymer, measured in chlorobenzene for  $R = C_{16}H_{33}$ . <sup>17</sup>  $1.81 \times 10^{-3}$  kcal/mol for CPDT-TQ polymer, measured in 1,2-dichlorobenzene for  $R = C_{12}H_{25}$ . <sup>6</sup>  $9.30 \times 10^{-3}$  kcal/mol for PhC=CPDT-TQ polymer, measured in 1,2 dichlorobenzene for  $R = C_{12}H_{25}$ .

Table 2. Summary OPA maxima ( $\lambda_{Max}$ , eV) for donor-acceptor decamers. Computed TD-B3LYP and TDA-OT-CAMB3LYP (in parentheses)  $\lambda_{Max}$  values were obtained using Gaussian line shape with FWHM of 0.4 eV.

	Theory	Experiment
System	$\lambda_{ ext{Max}}$	$\lambda_{Max}$
CPDT-BT (S)	1.26 (1.57)	1.73ª
PhC=CPDT-BT (S)	1.24 (1.55)	1.53 <sup>b</sup>
PhC=CPDT-BSe (S)	1.17 (1.47)	1.41 <sup>b</sup>
CPDT-BBT (T)	1.00 (1.11)	
PhC=CPDT-BBT (S,T)	1.00 (1.08)	1.01°
CPDT-TQ (S,T)	0.71 (0.79)	0.82 <sup>d</sup>
PhC=CPDT-TQ (T)	0.71 (0.76)	0.99 <sup>e</sup>
MAE <sup>f</sup>	0.24 (0.10)	

<sup>&</sup>lt;sup>a</sup>Measured in THF for  $R = C_{16}H_{33}$ . <sup>56</sup>

<sup>f</sup>Mean absolute error (MAE) and mean signed error (MSE): TD-B3LYP, 0.24 (-0.24) TDA-B3LYP, 0.19 (-0.19); sTDA-B3LYP, 0.34 (-0.34); sTDA-CAMB3LYP, 0.33 (0.33); TDA-(OT-B3LYP), 0.09 (-0.05); PCM-TDA-OT-CAMB3LYP, 0.11 (-0.08); TDA-PBE0, 0.13 (-0.10); sTDA-PBE0, 0.30 (-0.30). PCM calculations were carried out with the same solvents used in experimental measurements. See Table 4S for computed  $λ_{Max}$  values other functionals. Boltzmann average of three curve/spiral structures for: PhC=CPDT-BT, 1.24 (TD-B3LYP) and 1.55 (TDA-OT-CAMB3LYP). PhC=CPDT-BSe, 1.17 (TD-B3LYP) and 1.47 (TDA-OT-CAMB3LYP).

 $<sup>^{</sup>b}$ Measured in chloroform for R =  $C_{12}H_{25}$ .  $^{48}$ 

 $<sup>^{\</sup>circ}$ Measured in chlorobenzene for R =  $C_{16}H_{33}$ . <sup>17</sup>

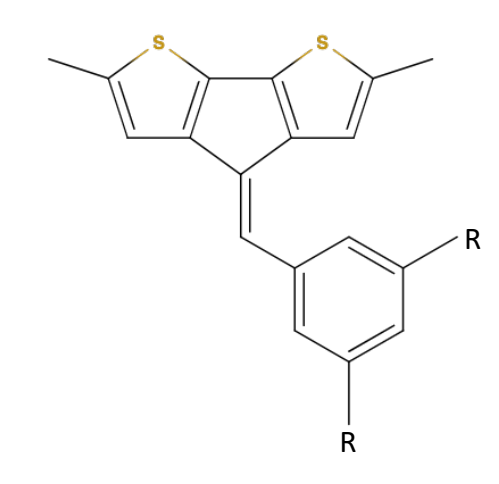
<sup>&</sup>lt;sup>d</sup>Measured in chloroform for  $R = C_{16}H_{33}$ .<sup>7, 18</sup>

<sup>&</sup>lt;sup>e</sup>Measured in 1,2 dichlorobenzene for  $R = C_{12}H_{25}$ .

a) Cyclopentadithiophene (CPDT)

c) Benzothiadiazole (BT)

e) Benzobisthiadiazole (BBT)



b) PhC=CPDT

d) Benzoselenadiazole (BSe)

f) Thiadiazoloquinoxaline (TQ)

Figure 1. Donor (a,b) and acceptor (c-f) molecular building blocks of oligomers.

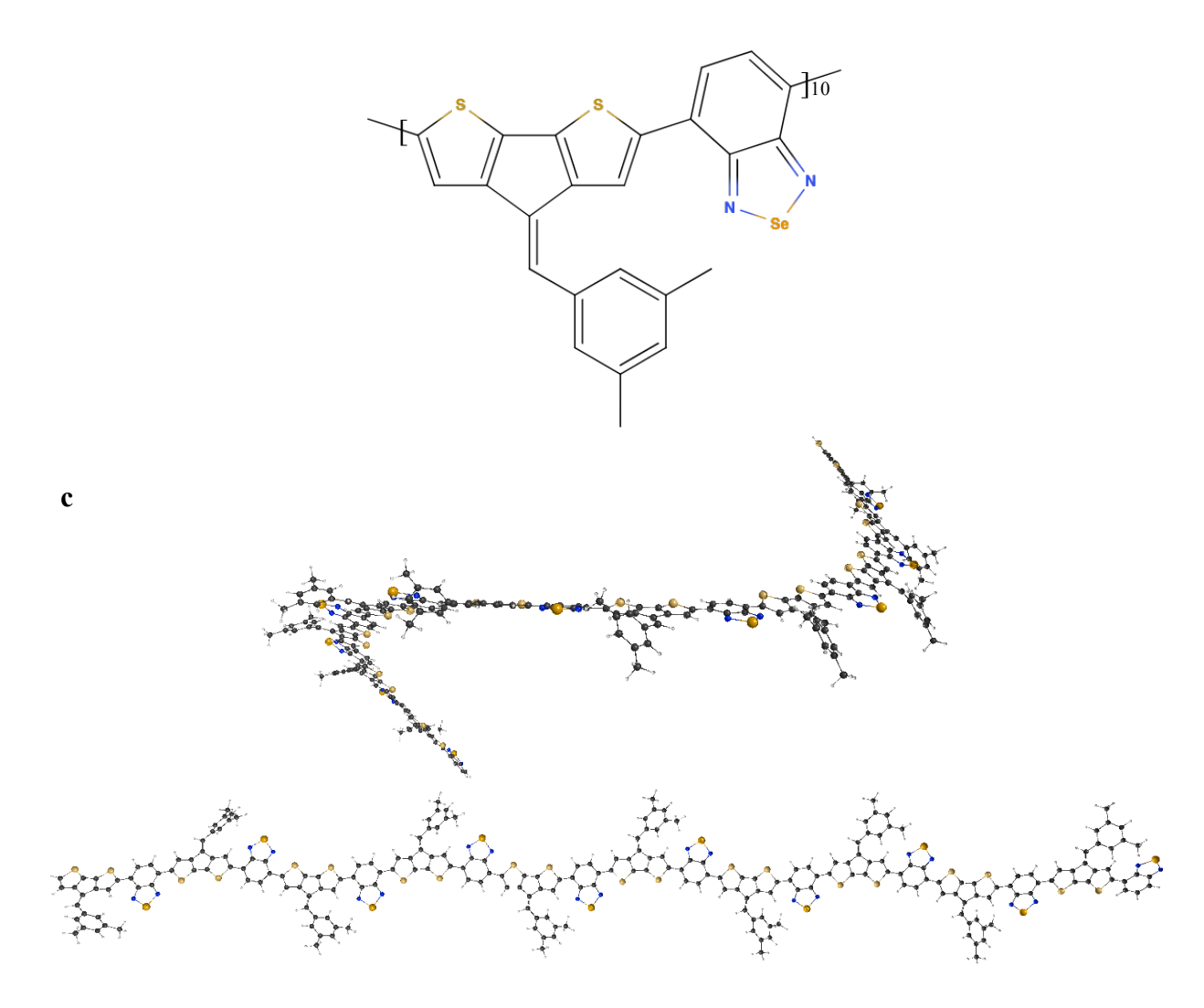


Figure 2. Curved and linear conformers for CPDT-BT (a), PhC=CPDT-BT (b), and PhC=CPDT-BSe (c) with 10 repeating units. The singlet curved structures are lower in energy by 6.7, 7.8, and 4.3 kcal/mol for CPDT-BT, PhC=CPDT-BT, and PhC=CPDT-BSe, respectively, compared to the linear counterparts.

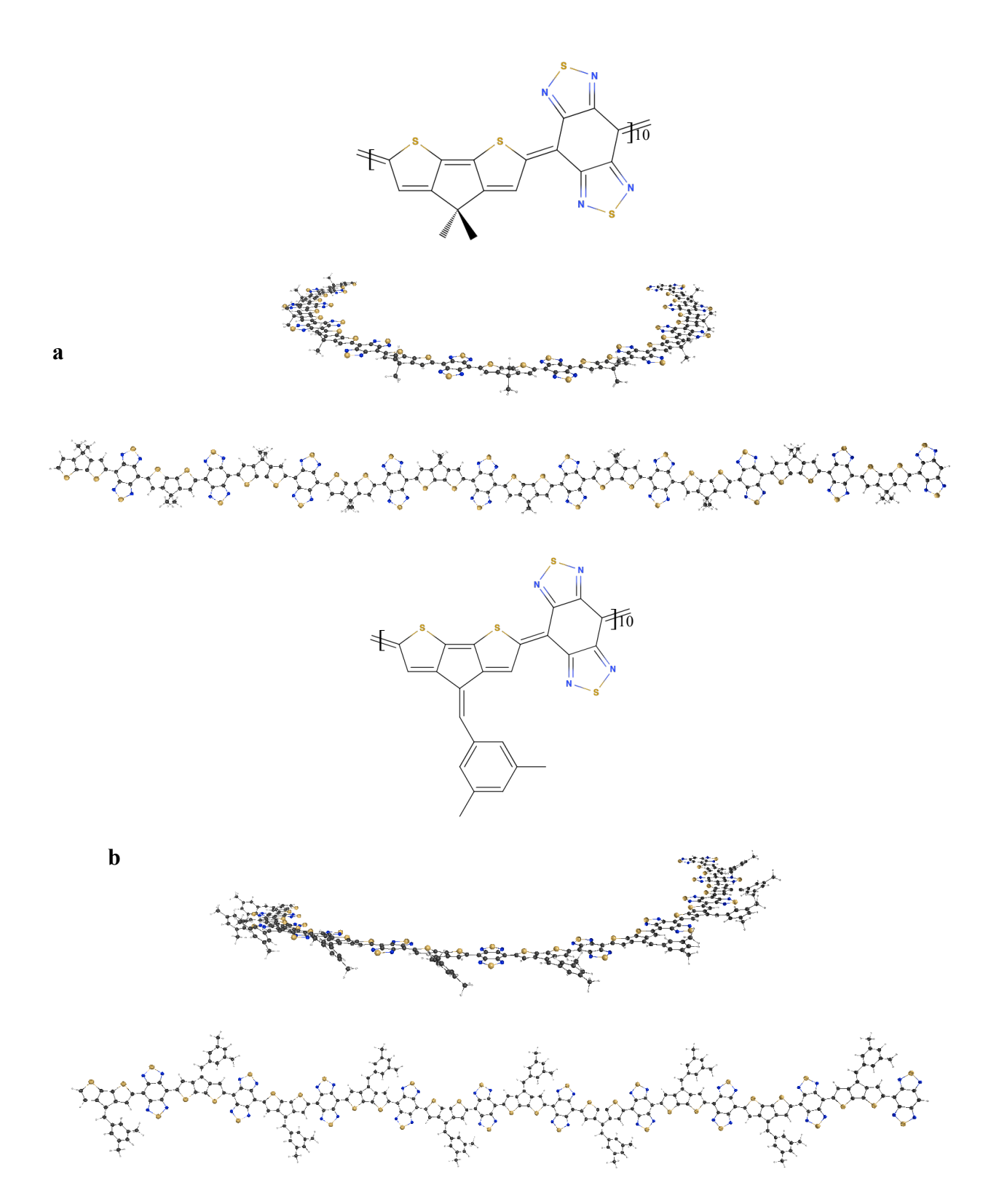


Figure 3. Curved and linear conformers for CPDT-BBT (a) and PhC=CPDT-BBT (b) with 10 repeating units. The triplet curved structures are higher in energy by 1.6 and 3.1 kcal/mol for CPDT-BBT and PhC=CPDT-BBT, respectively, compared to the linear counterparts.

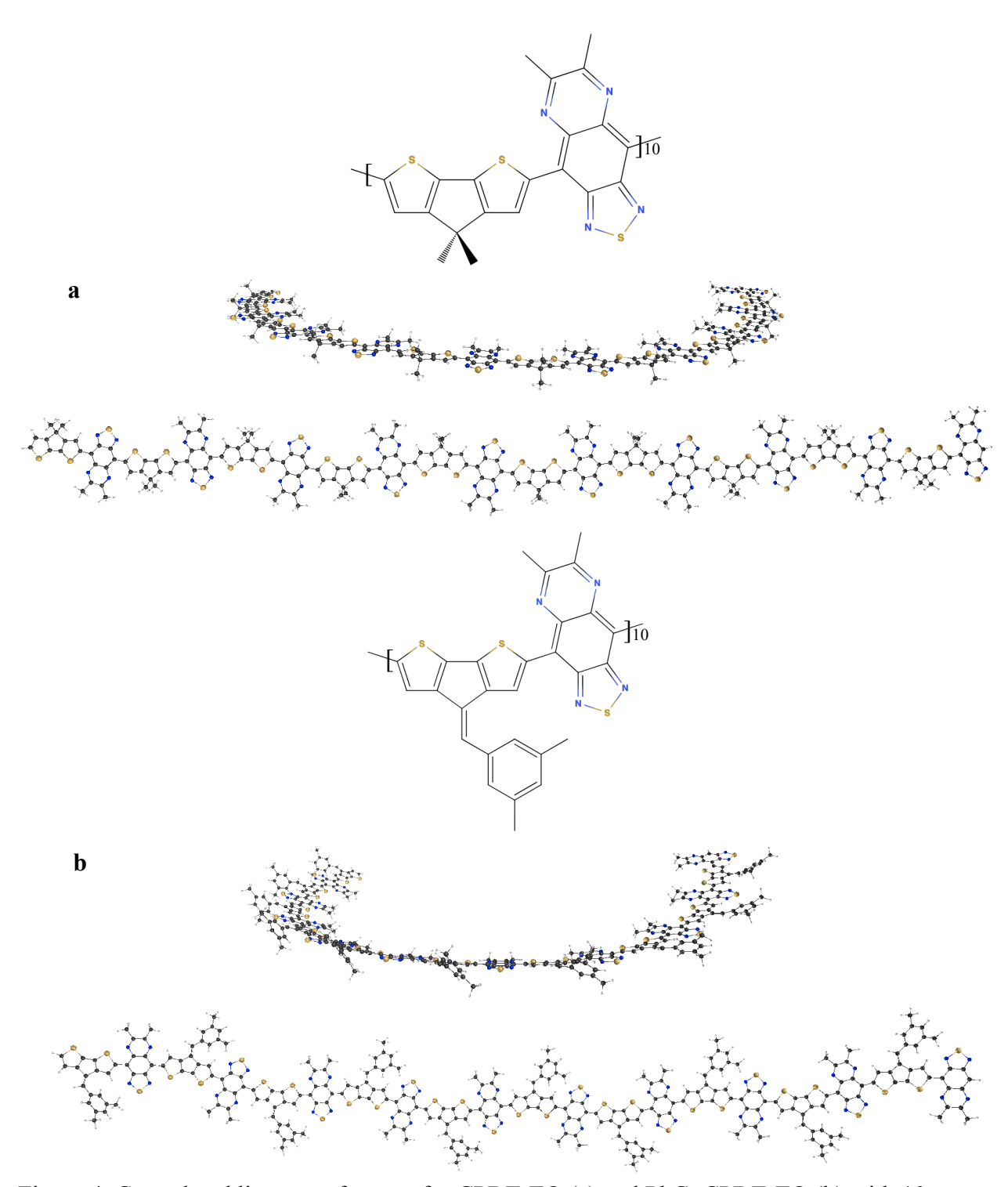


Figure 4. Curved and linear conformers for CPDT-TQ (a) and PhC=CPDT-TQ (b) with 10 repeating units. The triplet curved structures are lower in energy by 20.2 and 17.9 kcal/mol for CPDT-TQ and PhC=CPDT-TQ, respectively, compared to the linear counterparts.

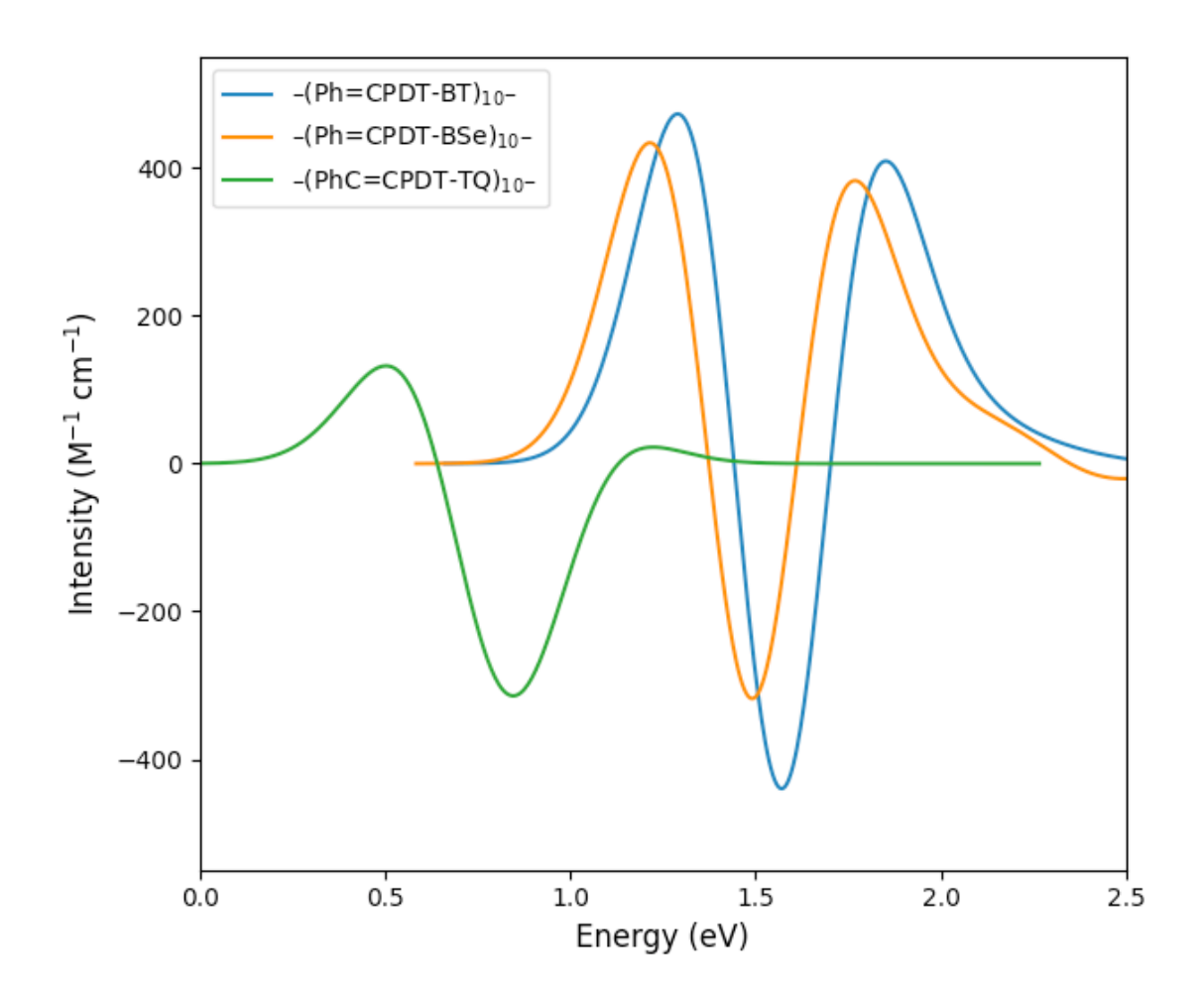


Figure 5. TDA-OT-CAMB3LYP ECD spectra for PhC=CPDT-BT, PhC=CPDT-BSe, and PhC=CPDT-TQ.

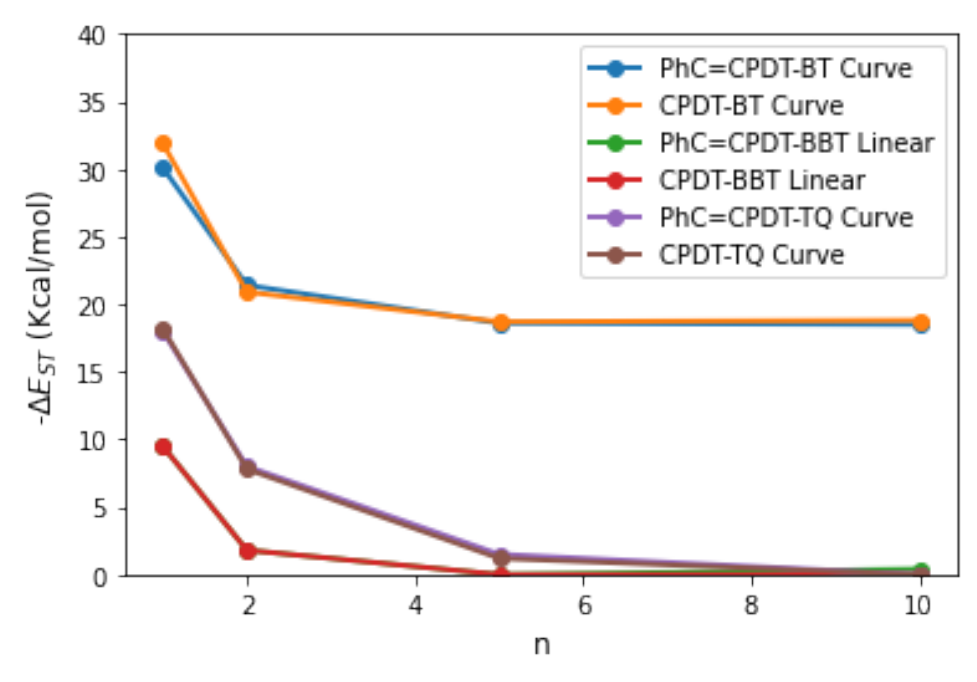


Figure 6. Gas-phase B3LYP-D3/6-31G(d,p) adiabatic singlet-triplet ( $\Delta E_{ST} = E_S - E_T$ ) gaps.

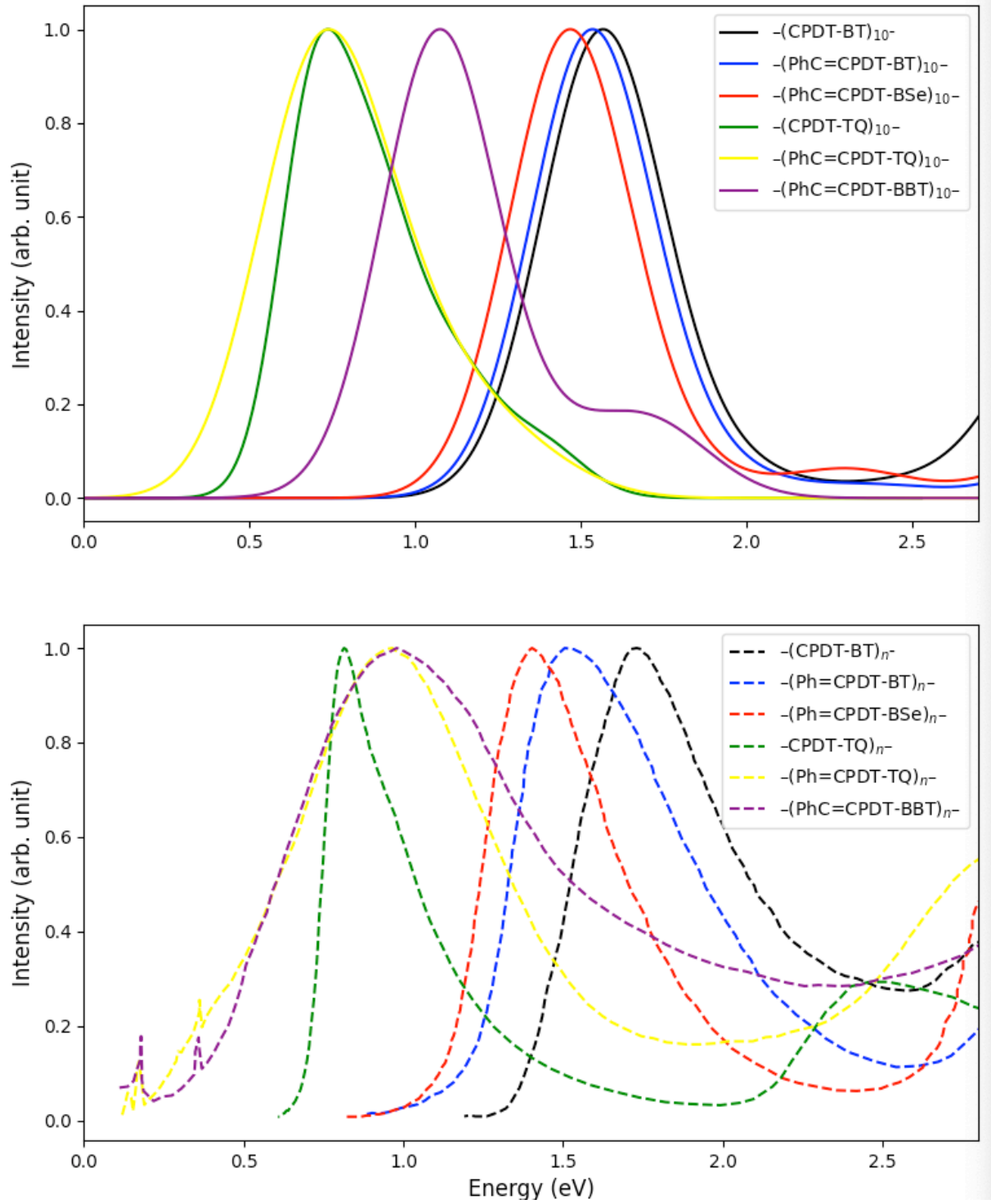


Figure 7. TD-OT-CAMB3LYP/6-31G(d,p) OPA spectra (top, using FWHM of 0.4 eV) compared to experiment (bottom).

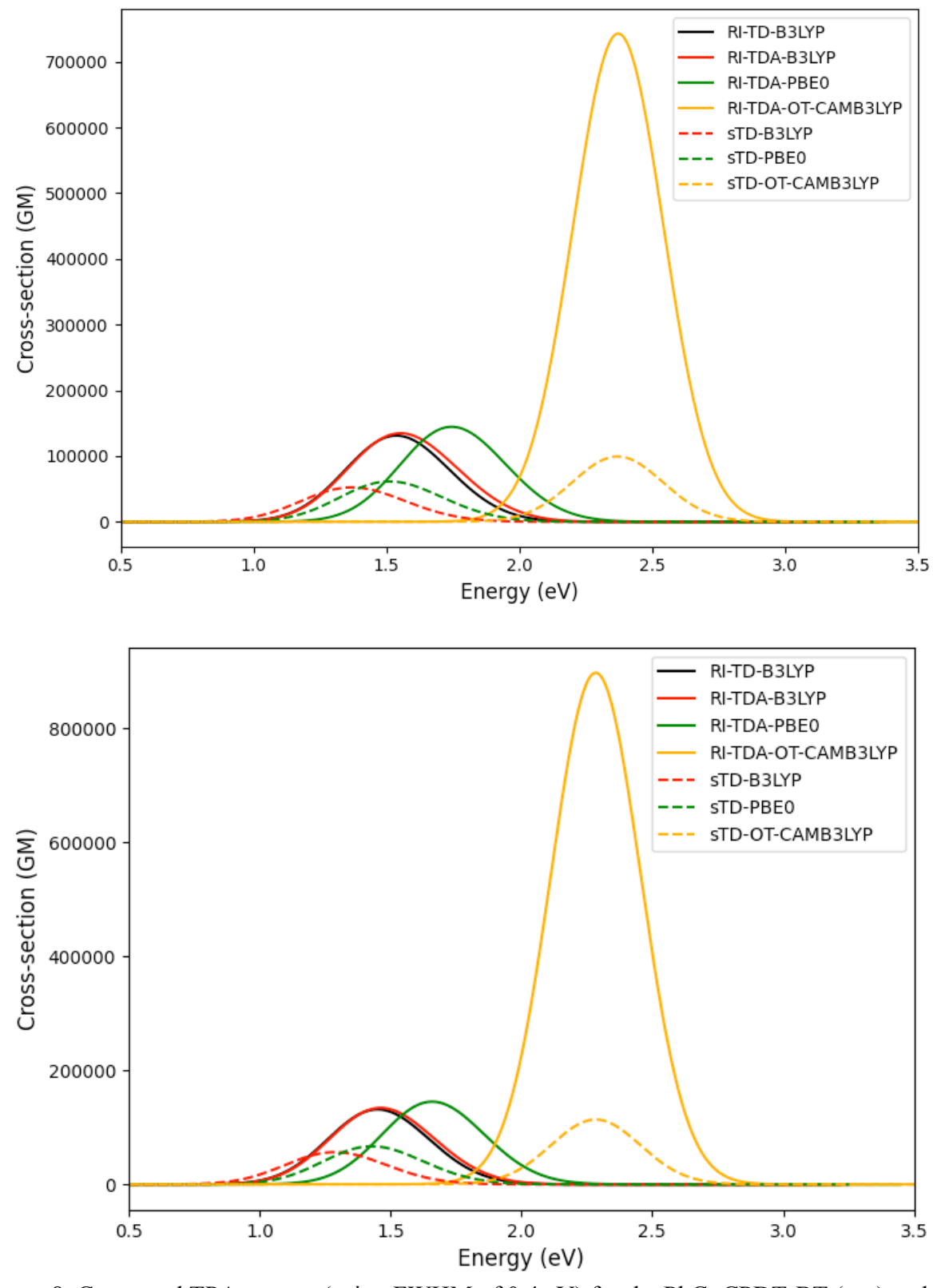


Figure 8. Computed TPA spectra (using FWHM of 0.4 eV) for the PhC=CPDT-BT (top) and PhC=CPDT-BSe (bottom) decamers.